https://doi.org/10.1016/j.tust.2020.103487

Deterioration Mapping in Subway Infrastructure using Sensory Data of GPR

Thikra Dawood[1], Zhenhua Zhu[2], and Tarek Zayed[3]

ABSTRACT

Water infiltration through soil is deemed the most serious problem and the main cause of concrete degradation in subway facilities. A huge amount of water intrusion may accelerate the deterioration mechanisms, such as rebar corrosion, spalling, and water voids. Such mechanisms can compromise the structural integrity and jeopardize public safety. The inspection and assessment of concrete structures are predominantly conducted based on visual inspection technologies. Although, these techniques may be consistent in detecting surface defects, e.g. cracks and spalling, they fall short in identifying subsurface distresses such as air voids, and water voids. Ground Penetrating Radar (GPR) has been extensively utilized for probing concrete infrastructure. Nevertheless, the deterioration mapping of air voids and water voids in concrete has seldom been performed. The objective of this paper is to develop an integrated model based on image processing of GPR profiles to automate air/water voids detection and mapping in subway systems. First, an automated localization scheme is developed to create a consistent inspection pattern. Second, subsurface data are collected in a subway facility, and processed using the image-based analysis technique. Third, the locations and dimensions of the detected defects are mapped to evaluate the severity of deterioration. The developed method is implemented on a tunnel in Montreal subway network. Then, validated via field inspection, digital images, coring samples, infrared thermography and 3D laser techniques. The validation outcomes reflect a strong correlation and compatibility with the generated GPR-based maps. The proposed framework is expected to assist infrastructure managers in identifying critical deficiencies and by focusing constrained funding on most deserving assets.

Keywords: Ground Penetrating Radar (GPR), Subway Networks, Inspection, Concrete, Deterioration, Air/Water Voids.

1. Introduction

[1] Postdoctoral Researcher, School of Construction Management , Knoy Hall of Technology, Purdue University, 401 N. Grant Street, West Lafayette, IN 47907-2021; Email: dawoodt@purdue.edu
[2] Mortenson Assistant Professor, Department of Civil and Environmental Engineering, Engineering Hall, University of Wisconsin-Madison, 1415 Engineering Drive, Madison, WI 53706; Email: zzhu286@wisc.edu
[3] Professor, Dept. of Building and Real Estate, Faculty of Construction & Environment, The Hong Kong Polytechnic University, ZN716 Block Z Phase 8, Hung Hom, Hong Kong; Email: tarek.zayed@polyu.edu.hk

Subway networks play a key role in the smart mobility of millions of commuters in major metropolises (Dawood et al. 2018). Transit ridership demonstrated an ascending trend in North America in the last decade and this trend is expected to continue (APTA 2016). According to the fourth quarter report of the American Public Transportation Association (APTA), in New York City, 2.8 billion trips took place in 2016, whereas in Toronto, that number reached around 303 million trips in the same year (APTA 2016). The integrity and durability of subway structures may be compromised due to severe environmental conditions, aging, and overloading capacity. The ASCE 2017 Report Card revealed that the condition of public transit infrastructure in the U.S. is rated D-; hence a rehabilitation backlog of $90 billion is estimated to improve transit status to good conditions (ASCE 2017). Moreover, the Canadian Urban Transit Association (CUTA) echoed the same message when it reported 74.9 billion CAD in infrastructure needs for the period 2018-2022 (CUTA 2019). Water intrusion through soil has been considered the most significant structural issue (Russell and Gilmore 1997; Chaussée 2012). The subway deterioration rate is accelerated as water infiltration increases, which might jeopardize the public safety. Other structural mechanisms are derived from water intrusion; among others are cracking, spalling, corrosion of reinforcing steel bars, and voids.

In hardened concrete (HC), an air void is a spherical or irregularly shaped air bubble that exceeds 1 mm in dimension and is contained in the cement paste. Generally, air void percentage is specified upon designing the mixture. It is recommended that a large number of very small air voids be produced in the paste so that proper air distribution is created through shortening the distance between air voids, hence protecting the paste from freezing and thawing cycles. A ratio of air void volume to paste volume that surpasses a specific limit may generate channel ways for the infiltration of water and the penetration of harmful substances, which may in turn, weaken the HC and affect its integrity. The compressive strength of concrete is lowered by around 5% for each excessive air void content (FHWA 1997). On the other hand, a water void is an irregular shaped pocket whose dimension surpasses 1mm. The unusually large amount of water voids found in fresh concrete indicates a defect caused either by craftsmanship or concrete mixture proportions. In subway networks, water voids are found behind concrete liners as a result of water infiltration through soil, which is considered the most serious problem and the main cause of concrete degradation, especially in subway networks constructed under rivers as the case in major metropolises (Chaussée 2012).

Faced with this litany of high deterioration rates, the pressure has increased on public transit authorities to develop automated tools and new strategies that tackle this critical safety issue; especially during the economic recession that minimized the funding policies. Therefore, providing cutting-edge serviceability through periodic structural inspection and assessment is crucial in keeping the subway network operational and avoiding catastrophic incidents. Such incidents cause the collapse of concrete infrastructure, which brings about fatalities and injuries, as well as the loss of wealth and businesses. One of these incidents has been reported on August 28, 1973 in Steinway Tunnel, one of the systems in New York City's subway network, when a delaminated upper slab fell and struck a Queens-bound IRT 11-car train. More than 1000 passengers were trapped in 115 degrees heat for over an hour. Subsequently, a fire was ignited due to a short circuit, creating smoke that impaired breathing and visibility. As a result, a 37-year old man died, and several others were hospitalized. This tunnel accident could have been avoided if adequate inspection and maintenance practices have been conducted in a timely manner (Russell and Gilmore 1997).

The condition assessment of metro structures is predominantly conducted on the basis of Visual Inspection (VI) techniques. While these techniques can deliver substantial inspection information (ACI 2008; Zhu and Brilakis 2010) about surface defects, e.g. cracks, spalling, etc., they have inherent shortcomings in recognizing and quantifying subsurface distresses, such as air voids and water voids (Abouhamad et al. 2017). Hence, such distresses cannot be diagnosed until they progress and become serious. The synergetic consequences of these mechanisms accentuate the need for a machine vision system that automates the current practice and provides consistent and objective outputs. This system utilizes the merits of GPR to remotely capture the profiles, processes and measures accurately the severity of distresses using multiple computational algorithms. Hitherto, there existed several models to evaluate the condition of concrete using the sensory data of GPR. Such models were tested on different civil structures; examples could be found in bridges (Maser and Bernhardt 2000; Benedetto et al. 2012; Lai et al. 2013; Tarussov et al. 2013; Hong et al. 2015; Romero et al. 2015). In pipelines (Ayala–Cabrera et al. 2013; Atef et al. 2015; Zhang et al. 2016). In pavements (Krysiński and Sudyka 2013; Liu and Sato 2014; Li et al. 2016b), and in tunnels (Lalagüe and Hoff 2010; Xiang et al. 2013; Baryshnikov et al. 2014). Nonetheless, there is a serious lack of GPR assessment models for subway structures, specifically; the identification and localization of air voids and water voids. The ultimate goal of this research is to propose a novel approach for automatically detecting and mapping air/water voids in subway systems using the sensory data of GPR. It endeavors to bridge the gaps in the body of knowledge and to ameliorate the existing level of subsurface assessment in concrete infrastructure.

2. Background review

2.1. GPR-based assessment models

A literature review revealed that there have been various endeavors to assess the Reinforced Concrete (RC) structures using the GPR. In this concern, Wiwatrojanagul et al. (2017) proposed an innovative method to determine the locations of reinforcement bars in concrete structures and quantify the cover thickness by using GPR data. Senin and Hamid (2016) estimated the moisture and chloride content in an RC slab by developing two nonlinear regression models. Subsequently, these models were compared to GPR amplitude attenuation data of the slab, which revealed good correlation results. Hoegh et al. (2015) characterized the air void variations in asphalt concrete using an air coupled GPR antenna to generate a dielectric map.

For bridge deck structures, Le et al. (2017) incorporated an autonomous robotic system with machine learning and pattern recognition techniques for efficient condition assessment of bridge decks. Their robotic system was equipped with a digital camera, GPR, and Electrical Resistivity (ER) for automatic scanning and profiles signal processing. Martino et al. (2016) developed a methodology to measure the bridge deck corrosion, by multiplying the mean and skewness of rebar attenuation signals of numerous bridge decks, then comparing the multiplication results to corrosion values measured by Half-Cell Potential (HCP) technique. While the technique developed by Martino et al. (2016) is easy to apply, it has not been tested in other infrastructure applications such as subway structures, nor to detect subsurface defects, e.g., air/water voids. This is due to the fact that their research was based on the signal attenuation recorded from corroded rebars, therefore, it cannot be applied to other than corrosion-induced defects, such as air/water voids in Montreal metro.

Dinh et al. (2015) clustered the GPR amplitude data into categories to assess the condition of concrete bridge decks. Their model was implemented and compared to the output of other NDE technologies, which confirmed reasonable results. Gucunski et al. (2015) devised a Robotics Assisted Bridge Inspection Tool (RABIT), which consisted of Impact Echo (IE), Electrical Resistivity (ER), Ultrasonic Surface Waves (USW) and GPR techniques. Thereafter, this fully autonomous tool was used to assess the delamination and concrete quality of bridge decks.

For pavements; Li et al. (2016_b) designed a pothole detector for concrete pavements subsequent to incorporating the image and GPR data processing. In another study, Li et al. (2016_a) computed the accuracy of a GPR method to evaluate the thickness of concrete pavements. Their method fused the outcomes of three NDE techniques; i.e., GPR, Impact Echo (IE), and Ultrasonic Surface Waves (USW). For tunnels; Prego et al. (2016) conducted a research to evaluate the capability of GPR in inspecting railway tunnels, specifically during the early phases of construction. The results revealed the appropriateness of GPR to evaluate the condition of concrete linings in tunnels. In the context of underground infrastructure; Atef et al. (2015) implemented a multi-tier technology to locate water pipes and detect their leaks after processing a myriad of images, acquired by Infrared (IR) and GPR techniques.

The previously-mentioned endeavors indicate that there still remain gaps in the body of knowledge, since the mainstream of GPR studies have focused on developing models based on the amplitude attenuation technique. This technique was found to be dysfunctional in the GPR profile analysis of non-reinforced elements of structures, because this analysis requires rebar picking to record the reflection amplitude of each rebar. Other GPR studies investigated subsurface defects, e.g., rebar corrosion, chloride content, moisture, and so forth. Nevertheless, little research work has been accomplished in locating and mapping of air voids and water voids in subway infrastructure. Especially, when these structures involve both reinforced and non-reinforced concrete.

2.2. Image-based analysis (IBA) of GPR profiles

Image-based analysis is an interactive procedure that is based on the visual recognition of predefined patterns in GPR profiles by a trained inspector. This procedure is achieved through a comprehensive learning process, which is based on understanding the structural aspects and configuration to visually diagnose the deterioration in GPR profiles (Dinh et al. 2013). The crucial clues and hypothesis behind the IBA has undergone continuous enhancements. Chung et al. (1992) employed a method grounded in the characteristic “W- shape” of GPR signals, in which any variation from the W-shape paradigm is deemed as indicative of some signs of deterioration.

Barnes and Trottier (2004) presented an efficiency study that relates the GPR with forecasting repair quantities of concrete bridge decks. Their model only reported coherent results when deterioration levels on the decks ranged 10% to 50%. Otherwise, substantial differences will be incurred between the GPR results and ground-truth quantities when the deterioration severity is less than 10% or more than 50%. To cope with this drawback, Tarussov et al. (2013) developed a functional approach for processing and analyzing GPR scans. In this approach and prior to the analysis process, a preprocessing phase is required to organize each profile into a two-dimensional grid. Thus, the coordinates and the amplitudes are corrected and optimized to be visually interpreted, while the proper differential gain is applied to the profiles. Then an experienced analyst scrolls through each GPR profile to determine the deteriorated zones by marking the severe zones in yellow and the very severe zones in red as illustrated in Fig. 1. While marking the zones, the analyst takes into consideration numerous factors, such as surface distresses, variations of rebar spacing, alignment, and depth, etc. The boundaries of the deteriorated zones marked in each GPR profile are automatically processed to generate a 2D plan map of the area using a specialized software.

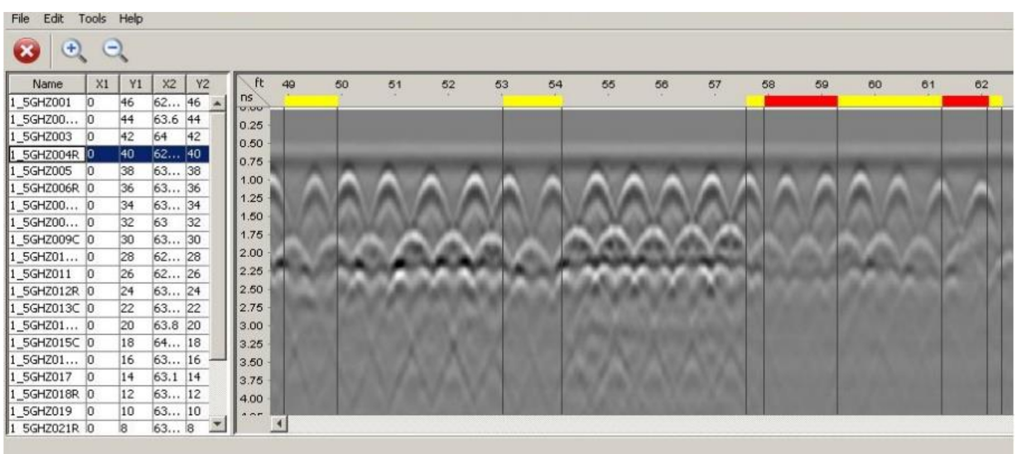

Fig. 1. Marking the deteriorated zones using IBA

The main advantage of IBA method is that it can identify both, the corrosion and non-corrosion related causes of signal attenuation, which is a significant merit that differentiates this method and characterizes it over the conventional numerical-amplitude analysis method (Abouhamad et al. 2017). Thus, the IBA is capable of diagnosing and mapping the distresses in the reinforced and non-reinforced concrete facilities. Whereas, the numerical-amplitude method can only detect and map the corrosion-induced damaged areas in concrete through investigating the variation of reflected amplitudes.

3. Research methodology

The proposed framework encompasses systematic approaches, which embark upon selecting the GPR for scanning the structure to accomplish the ultimate research goal of mapping air voids/water voids in subway systems. Prior to selecting the GPR, a comparative analysis is performed to select the most appropriate NDE technique for subsurface inspection. Such NDE techniques include infrared thermography, GPR, half-cell potential, acoustic methods, impulse response, impact echo, cover meter, ultrasonic pulse velocity, and spectral analysis of surface waves. Each technique is compared against eleven selection criteria, such as NDE capability to detect water infiltration, could be used as a stand-alone technique, rapidity of data collection and analysis, requires minimal human analysis, etc. Consequently, the comparison results show that GPR is superior to other techniques in accordance to each selection criterion. Therefore it is exploited to scan the structures of metro facilities. Fig. 2 illustrates the overall flowchart of the model architecture that includes three major steps; selecting the proper scanning antenna, data collection and profiles processing, and mapping the deteriorated concrete zones.

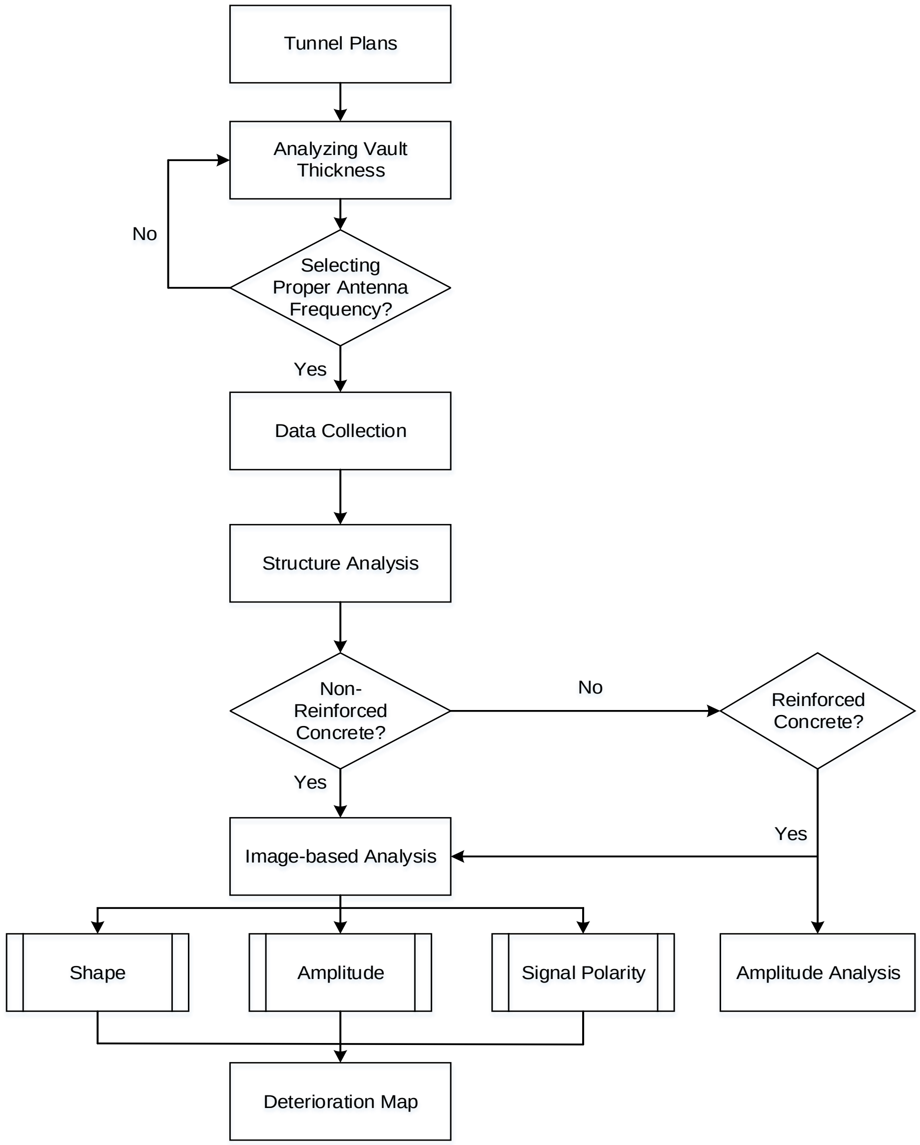

Fig. 2. Proposed model for air/water voids mapping

1) Selecting the proper scanning antenna

Attaining the best outcomes in analyzing GPR profiles hinges on selecting the proper GPR operating frequency that is literally the frequency bandwidth of GPR antenna. It controls the waves' penetration depth and spatial resolution. According to Annan and Cosway (1994), there is a trade-off between penetration depth, resolution, clutter reduction, and GPR mobility. It is recommended to trade-off spatial resolution for signal penetration depth since there is no benefit of attaining high resolution while the object cannot be detected. In general, the high frequency of the antenna will bring about high-resolution intensity, but low penetration depth. Therefore, tunnel plans are probed and analyzed to determine the component thickness in subway structure, thus allowing the selection of the ideal GPR antenna frequency.

2) Data collection and profiles processing

Data are collected for a segment of the component using the selected GPR antenna. Fig. 3 represents scanning the tunnel in a Montreal subway system via GPR. Prior to performing these surveys, a comprehensive plan is predetermined, which involves the number of inspectors, type of equipment, number of survey lines, scanned distance, etc. Accordingly, the data processing technique is specified based upon the reinforcement existence in the structure and types of distresses under investigation. Unlike the assessment of rebars' corrosion that necessitates applying the amplitude analysis technique; a procedure grounded in Image-Based Analysis (IBA) is proposed to identify and measure air/water voids zones in concrete components. This technique is based on the analyst's experience in the structure and his/her recognition of specific patterns in GPR profiles (Abouhamad et al. 2017).

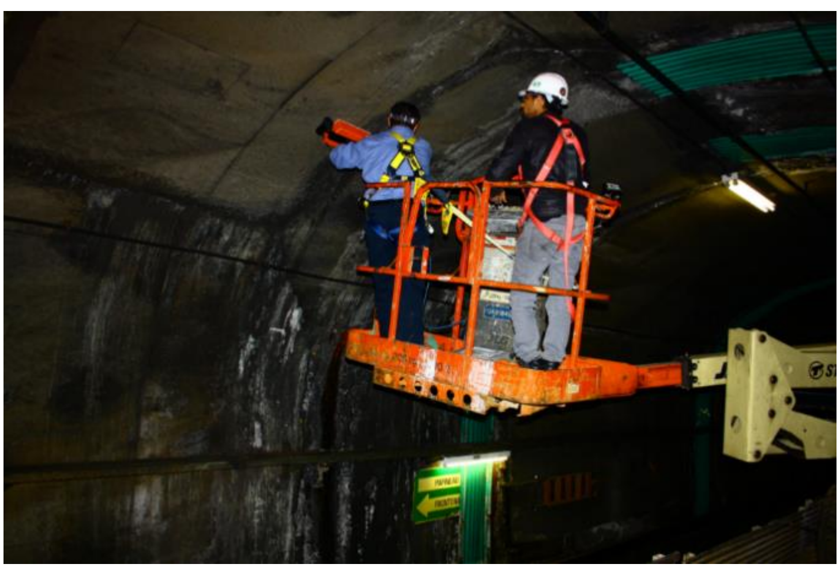

Fig. 3. Scanning a Montreal subway tunnel by GPR

The IBA starts with a preprocessing step that comprises organizing each profile into a 2D grid. Followed by adjusting the coordinates and signal amplitudes, while applying the differential gain to boost the visualization perception. Finally, a deterioration map for the structure is generated automatically during the processing phase using RADxpert® software. The general concept of the IBA of GPR profiles is explained in detail in Abouhamad et al. (2017). This paper focuses on the development of the IBA framework for the detection and mapping of air voids and water voids in concrete as illustrated in Fig. 4. The identification of voids defects in GPR profiles begins with checking the strength of the signal. The attenuation of the reflected signal indicates a probability of concrete deterioration. In the next step, structural elements and other anomalies are eliminated. The GPR data processing is conducted using a series of If-Then rules. This procedure is based on understanding the nature of the inspected structure, as well as, on the factors considered and/or eliminated for each GPR profile. The following represent the factors to be considered in this procedure:

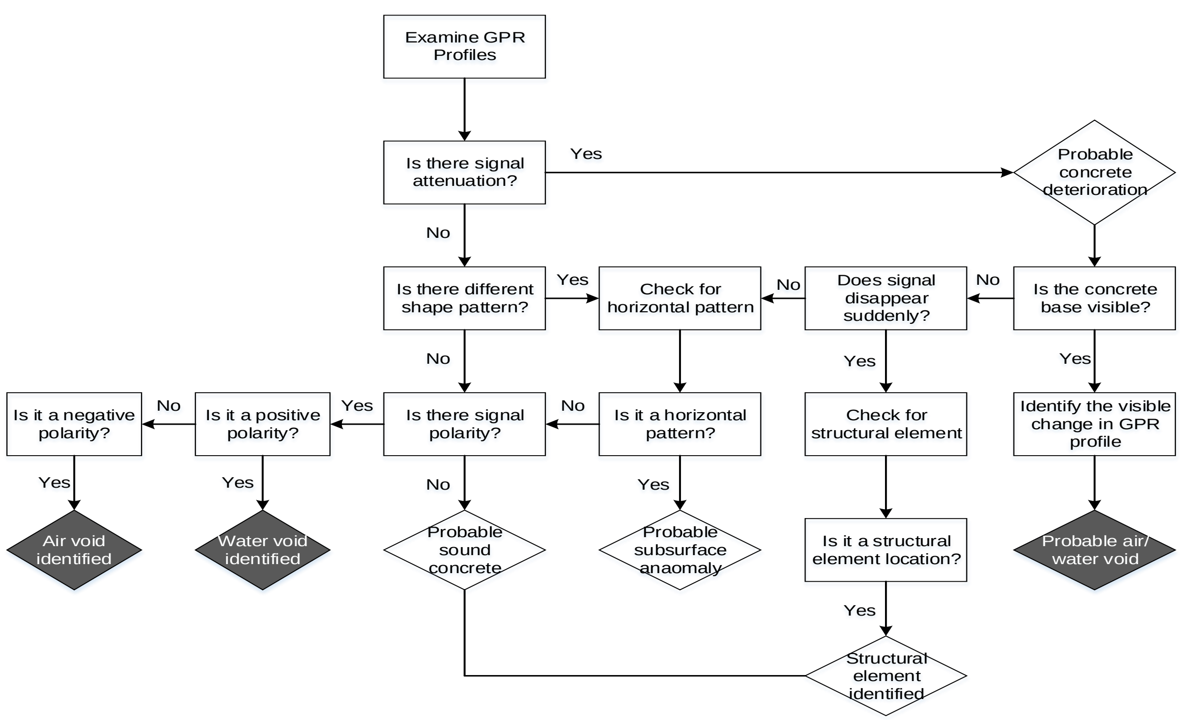

Fig. 4. Framework of air/water voids detection

a) Shape Pattern: In the IBA, the analyst scrolls each GPR profile and visually analyzes the signals. Once the analyst finds a distinct shape pattern, a thorough check for the pattern is performed. If it is a horizontal pattern, this indicates any anomaly in the concrete other than air/water void pocket, therefore it should be excluded from the analysis process. If the pattern displays a non-horizontal shape, it may possibly be an air/water void defect.
b) Wave Amplitude: As the beam of electromagnetic wave is transmitted through different materials, it will encounter an interface between two media of different dielectric constants, hence its amplitude will alter accordingly. The amplitude inversion is due to various causes. It might be an indication of a structural element such as a steel joint, or a deterioration in concrete, i.e., air/water voids, or any concrete distress.
c) Signal Polarity: Reflection polarity is a function of dielectric constant between two media, therefore, it can gauge and infer the subsurface condition. The dielectric constants of air, water, and concrete are quite distant from each other, as it is equal to 1 for air, 81 for water, and ranges 6-12 for concrete (Gehrig et al. 2004). Negative polarity occurs when the dielectric constant of layer 1 is more than the dielectric constant of layer 2 and vice versa. The signal polarity characteristic can provide tremendous benefits in detecting air/water voids in concrete infrastructure since the air void will display a negative (reversed) polarity, whereas a positive polarity will appear when there is a water void in the vicinity.

3) Mapping the deteriorated concrete zones

In the final step, GPR profiles can be consistently processed via the analysis software after marking the potentially deteriorated zones, i.e., air voids in yellow and water voids in red. It's worth noting that the unmarked zones on GPR profiles are the non-deteriorated areas of concrete, thus they signify the green probable sound concrete. The software will automatically process the previously marked zones and produce a deterioration map. The state of concrete can be classified into three categories based on the degree of signal attenuation in GPR profiles. Hence, in this perspective, there exist three hypotheses for the interpretation of GPR data: (a) probable sound concrete; (b) probable air void; and (c) probable water void. Table 1 identifies the various concrete states and their corresponding description. These three categories and their associated signal attenuation degrees were determined through a study conducted by Dinh (2014). In this study, a questionnaire survey was prepared and sent to the bridge and GPR experts in the US and Canada. The experts were asked to use a condition index scale for subsurface defects ranges from "0" to "100", with "0" representing the worst condition and "100" representing the excellent condition. In addition, they were provided with a three-color table, along with a description of the degree of signal attenuation, similar to Table 1. The goal was to link the linguistic descriptions and attenuation degrees with their associated colors, and to determine the values pertaining to the boundaries of each condition state. After analyzing the survey results, it was possible to derive the various concrete states and their corresponding description.

Table 1
Definition of different concrete states via IBA.

Probable Sound Concrete	**Probable Air Void**	**Probable Water Void**
Strong wave amplitude; there are no detected shape patterns or signal polarity.	Weak wave amplitude; there are visible shape patterns and negative signal polarity.	Strong signal attenuation; there are visible shape patterns and positive signal polarity.

4. Model implementation and results

The proposed framework was implemented on a vault inter Frontenac & Papineau Tunnel (FPTV). This tunnel is constructed in 1962 and is one of the systems on the Green Line of Montreal's subway networks. After shutting down the services in the tunnel, the first step was scanning the vault using the GSSI handheld GPR with antenna frequency of 900 MHz. This frequency range is intuitively justified in the perspective of air/water void detection in this tunnel. Since the vault thickness in the tunnel is around 0.61m, the 900 MHz antenna resolution is quite satisfactory for data collection as it offers a close-range penetrating depth of 0-1m.

Second, the antenna was mounted on a man lift that was attached to an inspection train to allow a smooth transition and high accuracy of subsurface scanning as shown in Fig. 3. Subsequent to adjusting the GPR setting and calibrating its antenna, surveys were performed for the tunnel vault in Montreal Metro. These surveys encompassed 14 parallel lines equally spaced 0.5 m apart, between 910.00 m and 886.20 chaînages in Montreal subway networks as represented in Fig. 5.

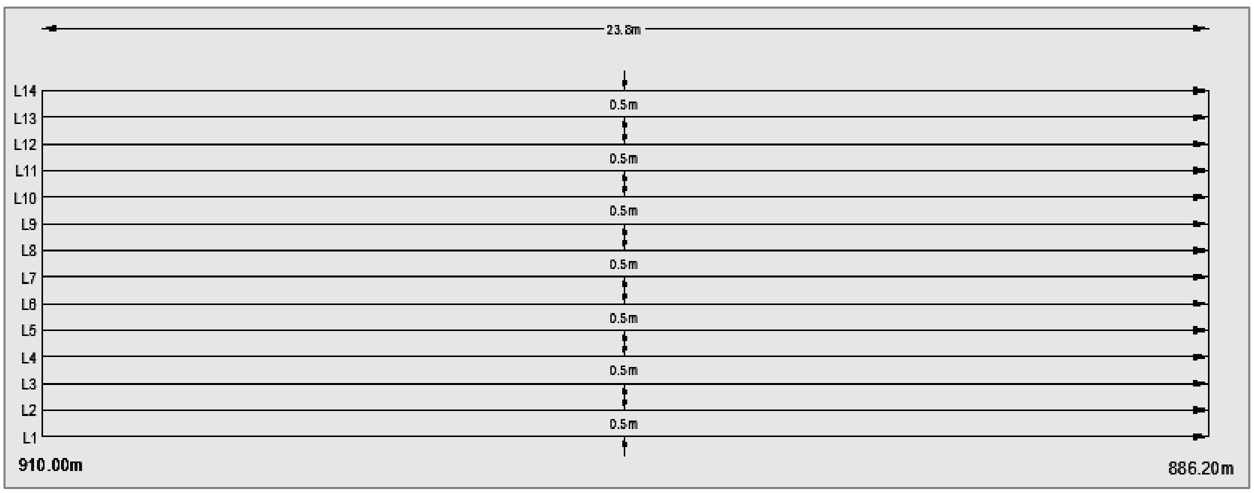

Fig. 5. Tunnel plan and scanning paths

The structure was scanned via a dual polarization technique. Using this technique, the structure is scanned once in the longitudinal direction, and in the second time in the transversal direction. The dual polarization technique is quite beneficial for probing huge structures such as subway systems inside which rebars are closely spaced, which render it hard to detect subsurface defects such as rebar corrosion by large antennas. Therefore, this technique offers a reasonable horizontal resolution to distinguish the anomalies in concrete.

Afterward, the framework of air/water voids detection, shown in Fig. 4 was implemented. The GPR profiles processing was conducted using a series of if-then rules based on the factors considered and/or eliminated, and based on the understanding of the nature of the studied structure.

The factors that were considered: (a) shape pattern; (b) wave amplitude; and (c) signal polarity. Therefore, each GPR profile was examined, by moving vertically in the flowchart to verify the abovementioned factors. If none of these factors is found, this is an indication of a probable sound concrete or a structural element existence. However, if there is signal attenuation, it means that the concrete is probably deteriorated. Given this scenario, there exist two options; first, the profile should be checked for any visible changes that are indicative of probable air/water void in the concrete. The second option, is to check if the signal disappears suddenly because this might be the location of a structural element, such as a supporting beam, as illustrated in the left side of Fig. 6.

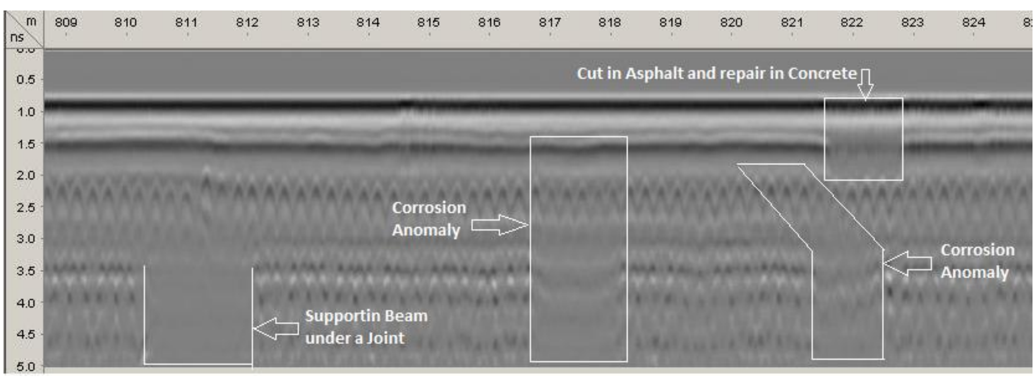

Fig. 6. Signal attenuation due to different anomalies and defects

In case that the signal is still clear and strong, next step is to search for a horizontal pattern as demonstrated in the lower GPR profile of Fig. 7. This pattern reflects the position of probable subsurface anomalies, i.e. rebar corrosion, cut in asphalt and repair in concrete, chloride penetration. Such anomalies must be eliminated from the IBA framework. On the other hand, if the pattern is not horizontal, the third factor should be investigated, which is the signal polarity. Testing this factor relies on two bodies of evidence; the positive polarity and the negative polarity. The positive polarity signifies that there is a water void in the vicinity, nonetheless, the air void will display a negative polarity. Consequently, the air/water voids were detected easily through an extensive learning process based on the analyst's experience in the structure under investigation. Fig. 7 shows processing a series of the tunnel's profiles through IBA.

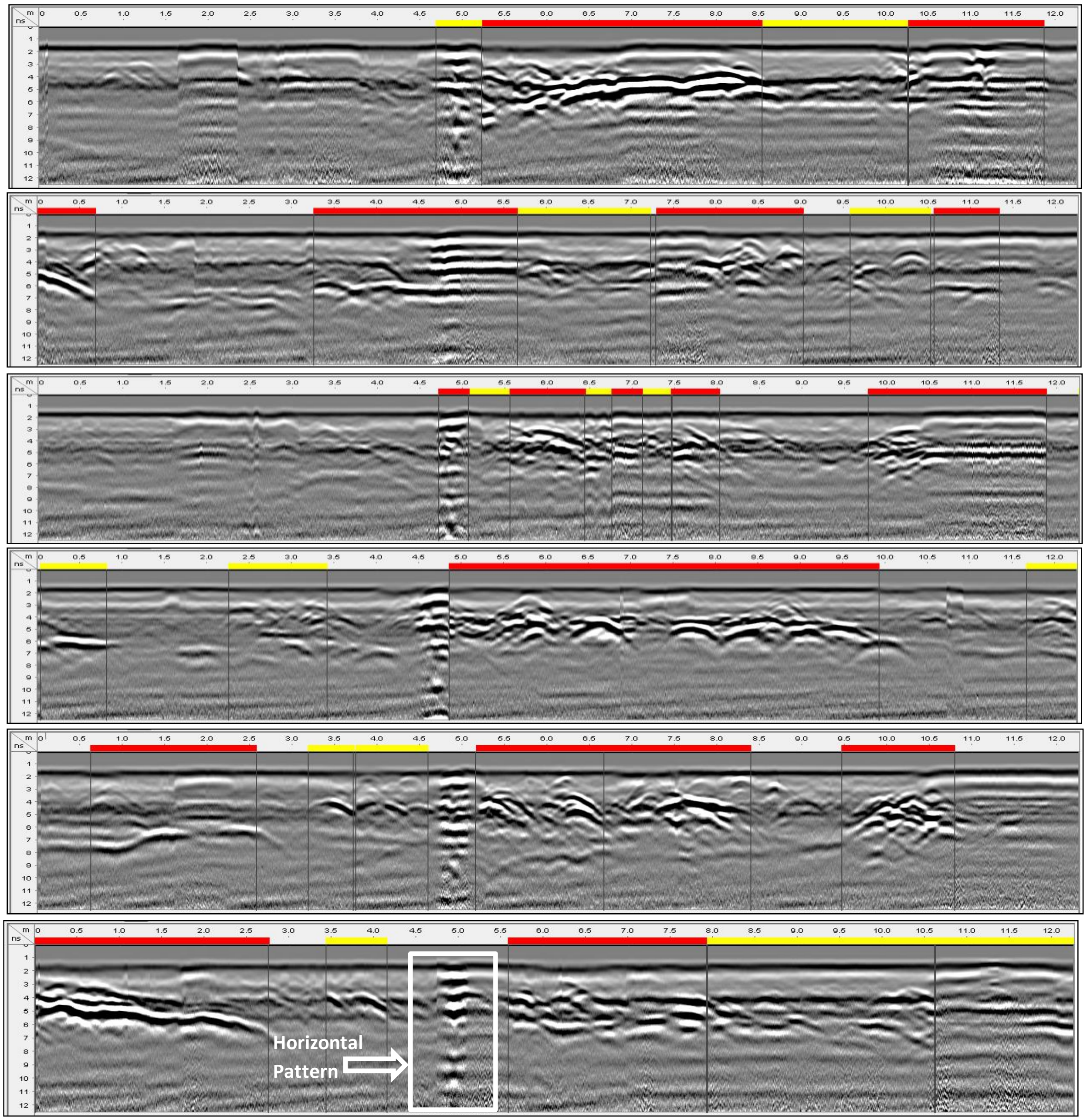

Fig. 7. Sample of processed GPR profiles via IBA

Finally, the GPR profiles were processed via the analysis software after marking the potentially deteriorated zones, i.e., air voids in yellow and water voids in red. The software processed the previously marked zones and generated the deterioration map of the tunnel vault automatically as depicted in Fig. 8.

The figure demonstrates that almost half the vault is found to be sound concrete as it is mapped in the green zone area, while the other half is located in the yellow and red zones where different elevations of probable air and water voids are in the vicinity.

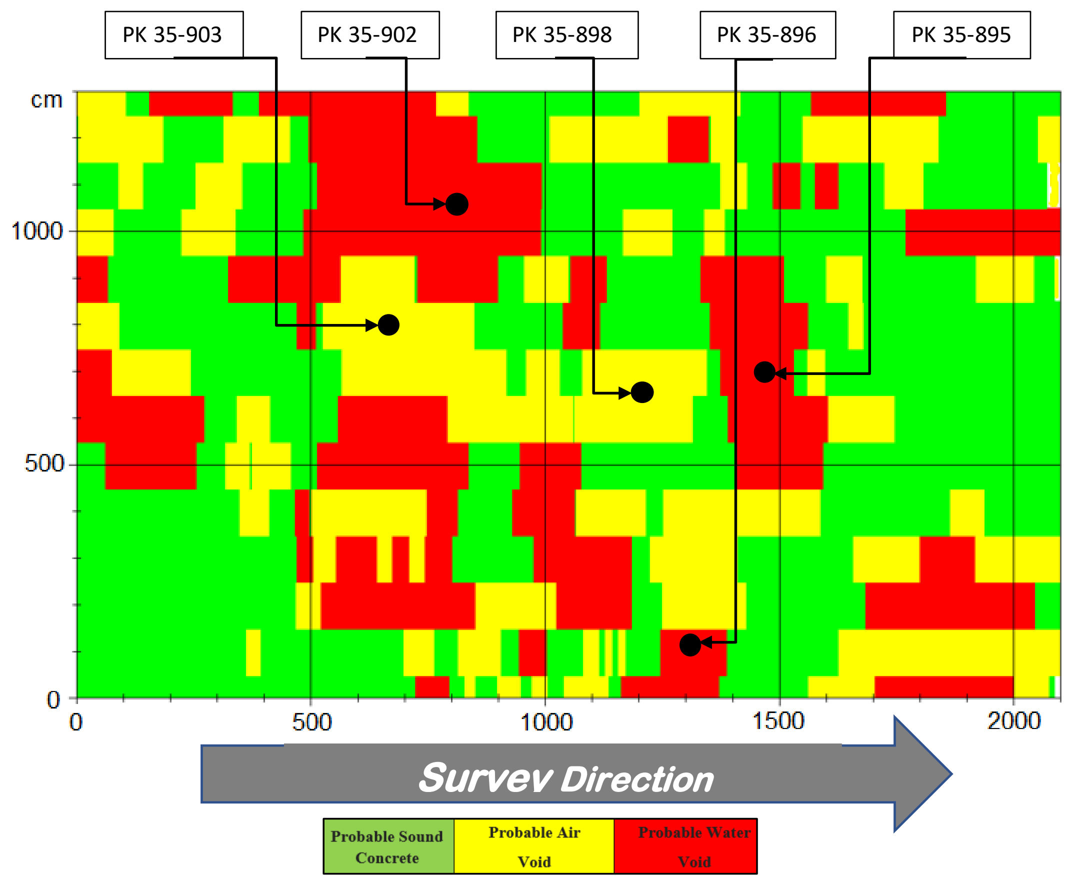

Fig. 8. Deterioration map of the tunnel vault

5. Model validation

The developed subsurface model of air/water voids using IBA was validated through various sensors and techniques. The advantage of combining different verification methods is that, such techniques can provide a comprehensive assessment of subsurface conditions all over the inspected area, not only at the selected locations. First, field inspection was undertaken to locate the healthy and damaged areas within the tunnel vault. In addition, camera images were captured at several locations of the vault to assure the robustness of the model. The correlation between the conditions provided by the GPR-IBA technique and the actual deterioration observed at different positions of the vault is apparent, as shown in Fig. 9.

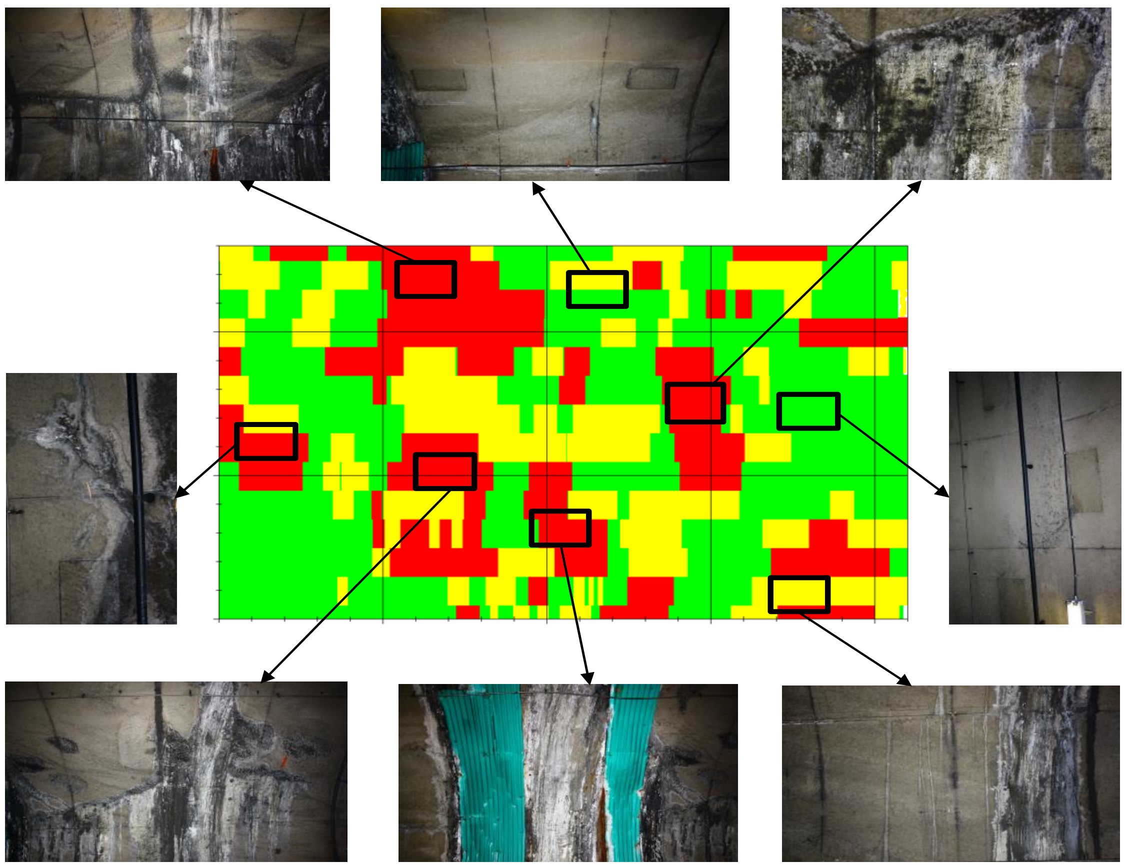

Fig. 9. Correlation between GPR-IBA and camera images in FPTV

Second, destructive tests were performed including ground truth core tests. Five locations were selected throughout the vault to execute core drilling work. Each core was coded for easy identification. Fig. 8 displays the coring positions in black dots along with their codes. Moreover, a cross section was obtained from each specimen in order to undergo a moisture content test using a digital moisture meter. The cores were extracted by using a hydraulic core drill that is water cooled. But, in order to prevent the water from confounding the moisture measurements, the drilling process was limited to only 10 minutes for each core. During this time the water cannot penetrate through the specimen and cause erroneous results, and since the coring was taking place in the vault, the water was dripping all through the process, which render it impossible to wetting the specimen. Table 2 summarizes the five samples and their properties. As demonstrated, coring test results of samples PK 35-902, PK 35-896, and PK 35-895 indicated high percentages of moisture content, recorded as 86, 74, and 65 respectively. These wet samples can also be noticed from their images and cross sections in Table 2. These results perfectly correlated with GPR-IBA for these three samples as located in the water void (red) zone on the map. While the moisture content percentages for samples PK 35-903 and PK 35-898 were found to be 22 and 19 respectively. Hence, they were categorized as dry samples, which correlated very well with GPR-IBA result and sited in the air void (yellow) zone on the map. Furthermore, examining the images and cross sections of these two samples in the table reflect dry areas.

Table 2
Coring samples and their properties.

Sample Code	**Depth (cm)**	**Moisture Content (%)**	**Sample Image**	**Cross Section**
PK 35-903	43.5	22		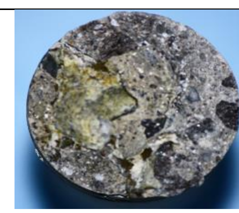
PK 35-902	40	86		

PK 35-898	38.5	19		
PK 35-896	40	74	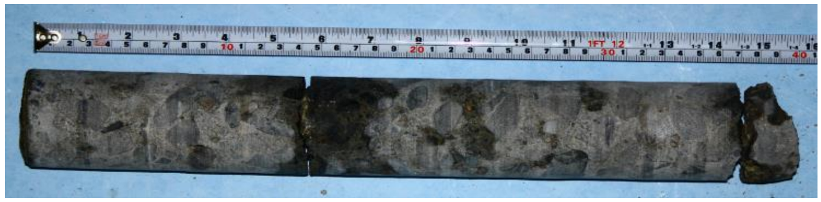	
PK 35-895	38	65	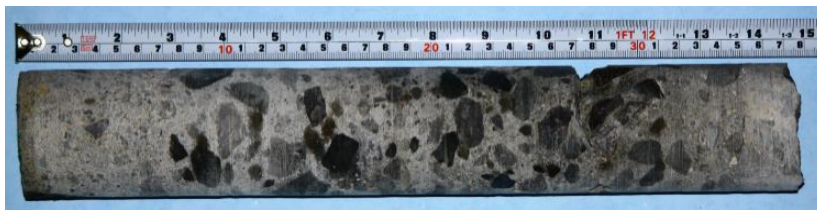	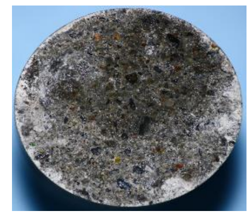

Third, additional NDE techniques such as infrared thermography (IR) and 3D laser scanner (LIDAR) were applied to further verify the results obtained from the proposed model and the designed tool. The Infrared camera (FLIR Zenmuse XT@MATRICE 100) with temperature range -40o to +550oC was applied to create a model for the tunnel. This approach utilized thermal and visible images to create a 3D point cloud model for the tunnel by performing the structure from motion method (Al Lafi et al. 2017). Next, overlapped thermal images were stitched in order to produce a panoramic image with precise temperature exemplification. Finally, thermal images were mapped to the 3D point cloud to enable measurements of subway tunnel components. Fig. 10(a) demonstrates the as-is laser-based thermal photo for the subway tunnel environment. When comparing the laser-based thermal map to the map generated using the IBA and shown in Fig. 10(b), a strong correlation between the two maps can be easily noted. The blue zones appearing on the laser-based thermal map indicate the cold areas according to the color visualization scale, which are the exact locations of water voids identified by the IBA. The validation outcomes reveal the feasibility of the developed model in terms of detecting air and water voids in metro systems.

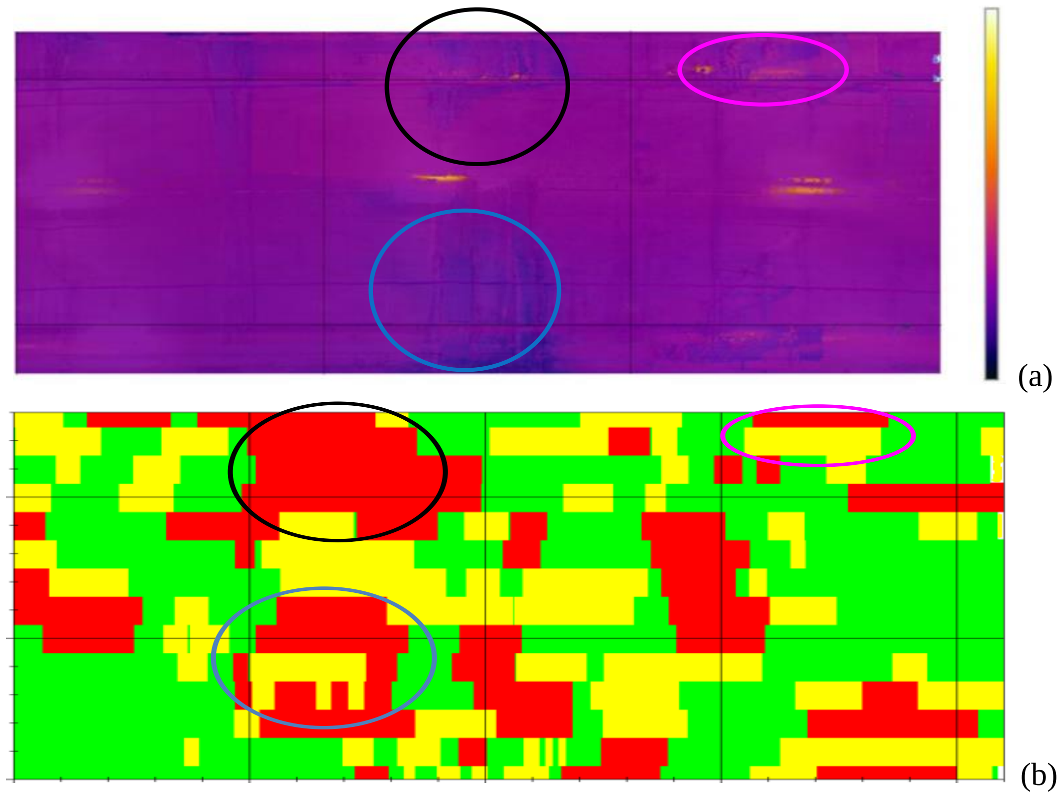

Fig. 10. Comparison between various NDE techniques. a – laser-based thermal ortho-photo (Al Lafi et al. 2017). b – GPR-IBA deterioration map

Moreover, the method developed by Huston et al. (2010) can be applied in order to perform quantitative correlations between the laser-based thermal map and GPR-IBA map. The method starts by mapping the raw data into values, and conducting a point-by-point comparison and a block-by-block comparison. Followed by calculating the Standard deviation of the data to confirm good agreement between the two maps. In addition to, computing the variance of the integrated condition estimations at each point. The low variance values indicate the zones of high correlation (Huston et al. 2010).

6. Summary and conclusions

This paper presented an integrated approach to detect and map air voids and water voids based on sensory data analysis of GPR. A comparative analysis was conducted to select the most appropriate NDE technology for subsurface inspection. As a result, the Ground Penetrating Radar (GPR) was superior to other methods according to the selection criteria. The GPR-based evaluation and deterioration mapping was realized through a three-tier methodology that entailed; selecting the proper scanning antenna, data collection and profiles processing, and mapping the deteriorated concrete zones. Several substantial aspects were taken into account throughout the Image-Based Analysis (IBA) framework, such as the visualized shape pattern in each profile, signal amplitude of the electromagnetic wave, and signal polarity. Subsequently, the proposed scheme was applied to a concrete tunnel in Montreal Metro. A deterioration map which delineates air/water voids zones in the tunnel was generated automatically. Moreover, the case study served to validate the proposed procedure, by leveraging different destructive and NDE technologies. The validation results revealed a strong correlation with the proposed methodology, which in return confirms the robustness and soundness of the model. This research contributes to the body of knowledge by enhancing the efficacy of air/water voids detection and mapping in metro infrastructure. It also proposes an Image-Based Analysis framework for the sensory data processing of GPR profiles. This framework offers transportation agencies a comprehensive strategy for the diagnosis and recognition of distresses in both the reinforced and non-reinforced concrete.

The only drawback of this model is its reliance on the analyst's knowledge and his/her visual interpretation of GPR profiles data. Future endeavors should address the enhancements to the current approach by developing an automatic processor, which measures the size and depth of voids in concrete structures. Other challenges need to explore a digital three-dimensional (3-D) information system that incorporates the photogrammetric and augmented reality (AR) techniques (Pereira et al. 2019). In this context, the photogrammetric and the GPR position registrations are integrated in order to locate the void and register its coordinates in a 3D manner, thereby elevating the coherence of the recent model by creating a 3D location map for underground structures.

7. Data availability statement

Data generated or analyzed during the study are available from the corresponding author by request.

8. Acknowledgments

The authors gratefully acknowledge Concordia University, Montreal, Canada (VE0119) & (VE0201); and the Natural Sciences and Engineering Research Council of Canada (NSERC) (N01811) for their financial support for this research. Any opinions, findings, conclusions, and recommendations expressed in this paper are those of the authors and do not necessarily reflect the views of Concordia University and NSERC.

9. References

Abouhamad, M., Dawood, T., Jabri, A., Alsharqawi M., and Zayed, T. (2017). "Corrosiveness mapping of bridge decks using image-based analysis of GPR data." *Automation in Construction*, 80, 104-117. http://dx.doi.org/10.1016/j.autcon.2017.03.004.

ACI (2008). *Guide for conducting a visual inspection of concrete in service*, ACI 201.1R-08, American Concrete Institute Committee 201, Farmington Hills, MI.

Al Lafi, G., Zhu, Z., Dawood, T., and Zayed, T. (2017). "3D thermal and spatial modeling of a subway tunnel: a case study." *Congress on Computing in Civil Engineering, Proceedings (ASCE)*, Seattle, WA, USA. 386-394. https://doi.org/10.1061/9780784480823.046.

Annan, A. P., and Cosway, S. W. (1994). "GPR frequency selection." *Proceeding of the Fifth International Conference on Ground-Penetrating Radar*, Kitchener, Ontario, Canada, 747-760.

APTA (2016). *American public transportation association ridership report- fourth quarter 2016*. Washington, D.C., USA. <http://www.apta.com/resources/statistics/Documents/Ridership/2016-q4-ridership-APTA.pdf> (June 15, 2017).

ASCE (2017). *2017 infrastructure report card*. American Society of Civil Engineering, https://www.infrastructurereportcard.org/cat-item/transit.

Atef, A., Zayed, T., Hawari, A., Khader, M., and Moselhi, O. (2015). "Multi-tier method using infrared photography and GPR to detect and locate water leaks." *Automation in Construction*, 61, 162-170. http://dx.doi.org/10.1016/j.autcon.2015.10.006.

Ayala–Cabrera, D., Herrera, M., Izquierdo , J., Oca˜na–Levario, S. J., and P´erez–Garc´ıa, R. (2013). "GPR-based water leak models in water distribution systems." *Sensors,* 13, 15912-15936. doi:10.3390/s131215912.

Barnes, C.L., and Trottier, J.F. (2004). "Effectiveness of ground penetrating radar in predicting deck repair quantities." *J. Infrastruct. Syst.*, 10 (2) 69–76, http://dx.doi.org/10.1061/(ASCE)1076-0342(2004)10:2(69).

Baryshnikov, V. D., Khmelin, A. P., and Denisova, E. V. (2014). "GPR detection of inhomogeneities in concrete lining of underground tunnels." *Journal of Mining Science,* 50(1), 25–32. https://link.springer.com/article/10.1134/S1062739114010049

Benedetto, A., Manacorda, G., Simi, A., and Tosti, F. (2012). "Novel perspectives in bridges inspection using GPR." *Nondestruct. Test. Eval.*, 27 (3) 239–251, http://dx.doi.org/10.1080/10589759.2012.694883.

Chaussée, D. (2012). "Montreal's subway system: challenges with an aging system." <https://www.icri.org/EVENTS/Spring12Present/16%20STM%20Montreal%20Subway%20System.pdf> (June 6, 2013).

Chung, T., Carter, C.R., Masliwec, T., and Manning, D.G. (1992). "Impulse radar evaluation of asphalt-covered bridge decks." *IEEE Trans. Aerosp. Electron. Syst.*, 28 (1) 125–137. http://dx.doi.org/10.1109/7.135439.

CUTA (2019). *2018-2028 Canadian Transit Infrastructure Needs.* Canadian Urban Transit Association, http://cutaactu.ca/sites/default/files/transit_infrastructure_needs_report.pdf.

Dawood, T., Zhu, Z., and Zayed, T. (2018). "Computer vision-based model for moisture marks detection and recognition in subway networks." *Journal of Computing in Civil Engineering*, 32(2). DOI: 10.1061/(ASCE)CP.1943-5487.0000728.

Dinh, K. (2014). "Condition assessment of concrete bridge decks using ground penetrating radar." Ph.D. Thesis, Concordia University, Montréal, QC., Canada.

Dinh, K., Zayed, T., and Tarussov, A. (2013). "GPR image analysis for corrosion mapping in concrete slabs." *Canadian Society of Civil Engineering 2013 Conference Proceedings*, 30, 1.

Dinh, K., Zayed, T., Moufti, S., Shami, A., Jabri, A., Abouhamad, M., and Dawood, T. (2015). "Clustering-based threshold model for condition assessment of concrete bridge decks using ground penetrating radar." *Transportation Research Record (TRR): Journal of the Transportation Research Board (TRB)*, 2522, 81-89. DOI: 10.3141/2522-08.

FHWA (1997). *Federal highway administration research and technology; coordinating, developing, and delivering highway transportation innovations*. Publication number: FHWA-RD-97-146.

Gehrig, M. D., Morris, D. V., and Bryant J. T. (2004). "Ground penetrating radar for concrete evaluation studies." *Technical Presentation Paper for Performance Foundation Association*, 197-200.

Gucunski, N., Kee, S-H., La, H., Basily, B., and Maher, A. (2015). "Delamination and concrete quality assessment of concrete bridge decks using a fully autonomous RABIT platform." *Structural Monitoring and Maintenance*, 2(1), 19-34. http://dx.doi.org/10.12989/smm.2015.2.1.019.

Hoegh, K., Khazanovich, L., Dai, S., and Yu, T. (2015). "Evaluating asphalt concrete air void variation via GPR antenna array data." *Case Studies in Nondestructive Testing and Evaluation*, 3, 27-33. https://doi.org/10.1016/j.csndt.2015.03.002.

Hong, S., Lai, W.L., and Helmerich, R. (2015). "Experimental monitoring of chloride-induced reinforcement corrosion and chloride contamination in concrete with ground-penetrating radar." *Struct. Infrastruct. Eng.*, 11 (1) 15–26. http://dx.doi.org/10.1080/15732479.2013.879321.

Huston, D., Cui, J., Burns, D., and Hurley, D. (2010). "Concrete bridge deck condition assessment with automated multisensor techniques." *Structure and Infrastructure Engineering*, 7 (7-8), 613-623. DOI: 10.1080/15732479.2010.501542.

Krysiński, L., and Sudyka, J. (2013). "GPR abilities in investigation of the pavement transversal cracks." *Journal of Applied Geophysics*, 97, 27–36. http://dx.doi.org/10.1016/j.jappgeo.2013.03.010.

Lai, W.L., Kind, T., Stoppel, M., and Wiggenhauser, H. (2013). "Measurement of accelerated steel corrosion in concrete using ground-penetrating radar and a modified half-cell potential method." *J. Infrastruct. Syst.*, 19 (2), 205–220, http://dx.doi.org/10.1061/(ASCE)IS.1943-555X.0000083.

Lalagüe, A., and Hoff, I. (2010). "Determination of space behind pre-cast concrete elements in tunnels using GPR." *Proceedings of the XIII Internarional Conference on Ground Penetrating Radar*, Lecce, Italy. DOI: 10.1109/ICGPR.2010.5550195.

Le, T., Gibb, S., Pham, N., La, H. M., Falk, L., and Berendsen, T. (2017). "Autonomous robotic system using non-destructive evaluation methods for bridge deck inspection." *IEEE International Conference on Robotics and Automation (ICRA)*, Singapore, Singapore. DOI: 10.1109/ICRA.2017.7989421.

Li, M., Anderson, N., Sneed, L., and Torgashov, E. (2016a). "Condition assessment of concrete pavements using both ground penetrating radar and stress-wave based techniques." *Journal of Applied Geophysics*, 135, 297-308. https://doi.org/10.1016/j.jappgeo.2016.10.022.

Li, S., Yuan, C., Liu, D., and Cai, H. (2016b). "Integrated processing of image and GPR data for automated pothole." *Journal of Computing in Civil Engineering*, 30(6), http://dx.doi.org/10.1061%2F(ASCE)CP.1943-5487.0000582.

Liu, H., and Sato M. (2014). "In situ measurement of pavement thickness and dielectric permittivity by GPR using an antenna array." *NDT&E International*, 64, 65–71. http://dx.doi.org/10.1016/j.ndteint.2014.03.001.

Martino, N., Maser, K., Birken, R., and Wang, M. (2016). "Quantifying bridge deck corrosion using ground penetrating radar." *Research in Nondestructive Evaluation*, 27(2), 112-124. http://dx.doi.org/10.1080/09349847.2015.1067342.

Maser, K., and Bernhardt, M. (2000). "Statewide bridge deck survey using ground penetrating radar." *Proceedings of Structural Materials Technology IV: An NDT Conference*, Atlantic City, NJ, pp. 31–37.

Pereira, M., Orfeo, D., Ezequelle, W., Burns, D., Xia, T., and Huston, D. R. (2019). "Photogrammetry and augmented reality for underground infrastructure sensing, mapping and assessment." *In International Conference on Smart Infrastructure and Construction 2019 (ICSIC) Driving data-informed decision-making*, pp. 169-175. ICE Publishing. DOI:10.1680/icsic.64669.169.

Prego, F. J., Solla, M., Núnez,-N. X., and Arias, P. (2016). "Assessing the applicability of ground-penetrating radar to quality control in tunneling construction." *J. Constr. Eng. Manage.*, 142(5). DOI: 10.1061/(ASCE)CO.1943-7862.0001095.

Romero, F.A., Barnes, C.L., Azari, H., Nazarian, S., and Rascoe, C.D. (2015). "Validation of benefits of automated depth correction method: improving accuracy of ground-penetrating radar deck deterioration maps." *Transp. Res. Rec.*, 2522, 100–109. http://dx.doi.org/10.3141/2522-10.

Russel, H.A., and Gilmore, J. (1997). *Inspection policy and procedures for transit tunnels and underground structures*, Transit Cooperative Research Program Synthesis 23, National Academy Press, Washington, D.C.

Senin, S. F., and Hamid, R. (2016). "Ground penetrating radar wave attenuation models for estimation of moisture and chloride content in concrete slab." *Construction and Building Materials*, 106, 659-669. https://doi.org/10.1016/j.conbuildmat.2015.12.156.

Tarussov, A., Vandry, M., and De La Haza, A. (2013). "Condition assessment of concrete structures using a new analysis method: ground-penetrating radar computer-assisted visual interpretation." *Constr. Build. Mater.*, 38, 1246–1254, http://dx.doi.org/10.1016/j.conbuildmat.2012.05.026.

Wiwatrojanagul, P., Sahamitmongkol, R., Tangtermsirikul, S., and Khamsemanan, N. (2017). "A new method to determine locations of rebars and estimate cover thickness of RC structures using GPR data." *Construction and Building Materials*, 140, 257-273. https://doi.org/10.1016/j.conbuildmat.2017.02.126.

Xiang, L., Zhou, H. l., Shu, Z., Tan, S. h., Liang, G. q., and Zhu, J. (2013). "GPR evaluation of the Damaoshan highway tunnel: A case study." *NDT&E International*, 59, 68–76. http://dx.doi.org/10.1016/j.ndteint.2013.05.004.

Zhang, P., Guo , X., Muhammat, N., and Wang, X. (2016). "Research on probing and predicting the diameter of an underground pipeline by GPR during an operation period." *Tunnelling and Underground Space Technology*, 58, 99–108. http://dx.doi.org/10.1016/j.tust.2016.04.005.

Zhu, Z., and Brilakis, I. (2010). “Machine vision-based concrete surface quality assessment.” *Journal of Construction Engineering and Management*, 136, 210-218. https://doi.org/10.1061/(ASCE)CO.1943-7862.0000126.